Icarus 209 (2010) 542–555

Contents lists available at ScienceDirect

Icarus

journal homepage: www.elsevier.com/locate/icarus

A three-parameter magnitude phase function for asteroids

Karri Muinonen [a,b,*], Irina N. Belskaya [c], Alberto Cellino [d], Marco Delbò [e], Anny-Chantal Levasseur-Regourd [f], Antti Penttilä [a], Edward F. Tedesco [g]

[a] University of Helsinki, Department of Physics, Gustaf Hällströmin katu 2a, P.O. Box 64, FI-00014 U. Helsinki, Finland
[b] Finnish Geodetic Institute, Geodeetinrinne 2, P.O. Box 15, FI-02431 Masala, Finland
[c] Astronomical Institute of Kharkiv National University, 35 Sumska Street, 61035 Kharkiv, Ukraine
[d] INAF – Osservatorio Astronomico di Torino, Strada Osservatorio 20, 10025 Pino Torinese, Italy
[e] UMR 6202 Laboratoire Cassiopée, Observatoire de la Côte d'Azur, BP 4229, 06304 Nice Cedex 4, France
[f] UPMC Univ. Paris 06, UMR 7620, BP3, 91371 Verrières, France
[g] Planetary Science Institute, 1700 E. Fort Lowell, Suite 106, Tucson, AZ 85719-2395, USA

ARTICLE INFO

Article history:
Received 20 June 2009
Revised 31 March 2010
Accepted 5 April 2010
Available online 19 April 2010

Keywords:
Asteroids
Asteroids, Surfaces
Asteroids, Composition
Photometry

ABSTRACT

We develop a three-parameter H, G_1, G_2 magnitude phase function for asteroids starting from the current two-parameter H, G phase function. We describe stochastic optimization of the basis functions of the magnitude phase function based on a carefully chosen set of asteroid photometric observations covering the principal types of phase dependencies. We then illustrate the magnitude phase function with a chosen set of observations. It is shown that the H, G_1, G_2 phase function systematically improves fits to the existing data and considerably so, warranting the utilization of three parameters instead of two. With the help of the linear three-parameter phase function, we derive a nonlinear two-parameter H, G_{12} phase function, and demonstrate its applicability in predicting phase dependencies based on small numbers of observations.

1. Introduction

The absolute magnitude is a fundamental astronomical parameter. According to its current definition, the absolute magnitude (H) of an asteroid is its mean apparent magnitude in the Johnson V band over a full rotation cycle (to account for the irregular shape of most asteroids that produces a periodic variation in brightness) when observed at 1 AU from both the Sun and the Earth, and at 0° solar phase angle.[1] That is, the absolute magnitude quantifies the intrinsic brightness of an asteroid. This brightness is determined by the asteroid's size (D, diameter in km)[2] and geometric albedo (p_V); the latter parameter, which is used to quantify the intrinsic reflectance of the surface, is related to surface composition and texture. The relation between the diameter, geometric albedo, and absolute magnitude is given by:

$$\log_{10} D = 3.1236 - 0.2H - 0.5\log_{10} p_V. \quad (1)$$

It is used in many practical applications, in particular when determining the albedo, given the size and the absolute magnitude (e.g., when the size has been determined from spacecraft or adaptive-optics imaging or from thermal radiometric observations) or, conversely, when deriving the size, when the albedo and absolute magnitude are known (as in the case of polarimetric determination of the albedo). Accurate albedos and diameters are important for a number of fundamental studies, e.g., the inventory and size distribution of the asteroid population and the albedo distribution within dynamical families (Cellino et al., 2009).

When dealing with real photometric data, determining H for a given asteroid reduces to determining its phase function. This is because the dependence on the distances from the Earth and Sun, being merely an inverse square relation, is trivially accounted for. However, the fact that H is defined at zero phase angle introduces complications since few asteroids are observed near zero phase angle. Indeed, many main-belt asteroids are not observed at phase angles <10°. Therefore, we must extrapolate from the phase angle of observation to 0° using what we know about the variation of the magnitude as a function of phase angle. This variation is mostly linear over a wide range of phase angles, but a nonlinear brightness surge takes place at small phase angles (roughly <7°). The origin of this so-called opposition effect is believed to be an interplay of shadowing and coherent-backscattering mechanisms (e.g., Muinonen et al., 2002).

* Corresponding author at: University of Helsinki, Department of Physics, Gustaf Hällströmin katu 2a, P.O. Box 64, FI-00014 U. Helsinki, Finland. Fax: +358 (0)9 19150610.
E-mail address: karri.muinonen@helsinki.fi (K. Muinonen).

[1] The solar phase angle (generally shortened to "phase angle") is the angle between the Sun and the Earth as seen from the object.

[2] D is the diameter of a sphere having the same projected surface area as the asteroid.

0019-1035/$ - see front matter © 2010 Elsevier Inc. All rights reserved.
doi:10.1016/j.icarus.2010.04.003

To address this issue, in 1985, Commission 20 of the International Astronomical Union adopted the so-called H, G magnitude system (the Johnson V band at mean lightcurve brightness and the H, G phase function) to define asteroid absolute magnitudes. The two parameters of the H, G phase function have the following meaning: H corresponds to the mean brightness, in Johnson V magnitude, at 0° phase angle (i.e., the absolute magnitude), and G is the so-called slope parameter, which describes the shape of the magnitude phase function. In practice, the slope parameter has been derived for $\ll$0.1% of the known asteroids ($\lesssim$100 from the Minor Planet Center's orbital-elements file and perhaps a score of others mostly from asteroid lightcurve studies). In general, only a handful of photometric observations, obtained at only a few phase angles, are available for any given asteroid, and this is insufficient to derive both H and G. In these cases, an assumed value of G, usually 0.15, is adopted (Bowell et al., 1989). Since the shape of the phase function is determined by G, this allows for the derivation of H from magnitudes at as few as one phase angle. When observations from multiple phase angles are available the resulting H values are averaged. To some extent this increases the reliability of H by taking into account brightness variations due to lightcurve and aspect[3] effects.

The accuracy of V-band magnitudes predicted from available H, G values is usually poor, probably due to low-quality photometry used to obtain the H (and in a few cases, the G) values. The reason for this is that the vast majority of available asteroid photometry is from near-Earth-object search programs conducted over the past 15 years. Because these are discovery surveys, most of which obtain images using unfiltered CCDs, the emphasis is on limiting magnitude, sky area covered per unit time, and astrometric accuracy. In particular, for most surveys the "photometry", where it is provided at all, is not in the Johnson V band (or in any other standard photometric system) and does not use standard stars from photometric catalogs for calibration. Thus, it is not surprising that there is poor agreement between observed V magnitudes and those predicted using H, G values from the orbital-element catalogs all of which currently (except the AstDys database maintained by A. Milani at the University of Pisa) trace their values to the Minor Planet Center's database, the sole repository for H, G values recognized by the IAU. See Jurić et al. (2002), Jedicke et al. (2002), and Parker et al. (2008) for further discussions of this issue.

In practice, there are at least three accuracy levels required for H: (1) On the order of a few hundredths of a magnitude for detailed physical studies,[4] e.g., shape determination and thermophysical modeling, (2) ~0.1–0.2 mag for "statistical" physical studies, e.g., Durda et al. (1998), Tedesco et al. (2002a,b), Tedesco and Desert (2002), and Tedesco et al. (2005), and (3) ~0.2–0.5 mag for astrometric studies, e.g., for planning follow-up observations. Our work focuses on improving H for uses (1) and (2) by developing improved asteroid phase functions. In particular, as shown below, these new phase functions derive from basis functions that were originally determined using results from the best light-scattering models available, and which have been tested using the best magnitude phase curves available. We also demonstrate how a nonlinear two-parameter version of the linear three-parameter phase function can be used to predict asteroid brightnesses from sparse observational data and will provide an estimate of the accuracies to be expected for observations from various phase-angle ranges.

In Section 2, we review the H, G magnitude phase function, describe the stochastic optimization methods for deriving new phase functions, and summarize the error estimation of parameters using Monte Carlo methods. Section 3 describes the minimum-change effort for optimizing the H, G magnitude phase function, the derivation of the H, G_1, G_2 phase function, as well as the least-squares analyses of a set of observed phase curves. Based on the new three-parameter phase function, we derive a nonlinear two-parameter H, G_{12} phase function, and demonstrate the predictive power of the nonlinear phase function. Conclusions and future prospects close the article in Section 4.

2. Theoretical and numerical methods

2.1. H, G magnitude phase function

The H, G phase function for asteroids can be described as follows. If we call α the phase angle, and $V(\alpha)$ the V magnitude (reduced to unit distance) expected for an object characterized by given values of H and G, the following relation holds:

$$V(\alpha) = H - 2.5\log_{10}[(1-G)\Phi_1(\alpha) + G\Phi_2(\alpha)], \tag{2}$$

where $\Phi_1(\alpha)$ and $\Phi_2(\alpha)$ are two basis functions normalized at unity for $\alpha = 0°$. According to Eq. (2), the magnitude phase curve (hereinafter, "phase curve") of an object is described as the partitioning of the Φ_1 and Φ_2 functions in the ratio $(1-G)$:G. In turn, the slope parameter G is scaled in such a way that it is close to 0 for steep phase curves, and close to 1 for shallow phase curves, but values outside this interval are not excluded *a priori*.

In the H, G magnitude phase function for asteroids, the reduced observed magnitudes $V(\alpha)$ can be obtained from

$$\begin{aligned} 10^{-0.4V(\alpha)} &= a_1\Phi_1(\alpha) + a_2\Phi_2(\alpha) \\ &= 10^{-0.4H}[(1-G)\Phi_1(\alpha) + G\Phi_2(\alpha)], \end{aligned} \tag{3}$$

where the absolute magnitude H and the coefficient G are[5]

$$H = -2.5\log_{10}(a_1 + a_2), \quad G = \frac{a_2}{a_1 + a_2}. \tag{4}$$

The coefficients a_1 and a_2 are estimated from the observations by using the linear least-squares method. Thereafter, H and G follow from Eq. (4). In the H, G phase function, the basis functions are

$$\begin{aligned} \Phi_1(\alpha) &= w\left(1 - \frac{0.986\sin\alpha}{0.119 + 1.341\sin\alpha - 0.754\sin^2\alpha}\right) \\ &\quad + (1-w)\exp\left(-3.332\tan^{0.631}\frac{1}{2}\alpha\right), \\ \Phi_2(\alpha) &= w\left(1 - \frac{0.238\sin\alpha}{0.119 + 1.341\sin\alpha - 0.754\sin^2\alpha}\right) \\ &\quad + (1-w)\exp\left(-1.862\tan^{1.218}\frac{1}{2}\alpha\right), \\ w &= \exp\left(-90.56\tan^2\frac{1}{2}\alpha\right). \end{aligned} \tag{5}$$

These functions are accurately approximated by

$$\begin{aligned} \Phi_1(\alpha) &= \exp\left(-3.33\tan^{0.63}\frac{1}{2}\alpha\right), \\ \Phi_2(\alpha) &= \exp\left(-1.87\tan^{1.22}\frac{1}{2}\alpha\right). \end{aligned} \tag{6}$$

The two functions in Eq. (5) constituted the state of the art at the epoch of development of this photometric phase function. Their forms were suggested by theoretical models of light scattering that at that epoch did not yet include the phenomenon of coherent backscattering. Of course, the H, G phase function was developed and tested by means of a detailed analysis of the best

[3] The "aspect angle" is the angle between the asteroid rotation axis and the line of sight.

[4] In which case, to account for aspect variations, observations over several different apparitions are required.

[5] There is a misprint in Bowell et al. (1989) in the definition of the G parameter.

phase curves available at that time. Phase curves extending up to large phase angles were available for the Moon and Mercury. The database of asteroidal observations included phase curves for the objects (24) Themis, (44) Nysa, (69) Hesperia, (82) Alkmene, (133) Cyrene, (419) Aurelia, and (1862) Apollo (the only asteroid for which data at phase angles larger than 30° were available at the time). Due to the peculiarity of the Mercury phase curve at large phase angles, it was excluded from the development of the H, G phase function. The lunar phase curve was included in the development except for the observations at large phase angles $\alpha \geqslant 120°$.

More than 20 years since its adoption, there are reasons to try and improve the H, G phase function. This function still does a reasonably good job in fitting phase curves for many asteroids, especially in the region from ~10° to ~60°. However, there exist some high-quality phase curves for which this is not true, especially in the region of the opposition brightness surge.

This problem is not too serious in many practical cases, in particular, when trying to derive the absolute magnitude of asteroids for which only a few observations are available, in which cases the uncertainty in the derived absolute magnitude is not due to the adopted phase function, but rather to the quality, quantity, and distribution over phase angle of the data. Nevertheless, an optimal phase function should provide accurate fits to high-quality data, and this is not always true for the current version of the H, G phase function.

Before proceeding to describe revising the H, G phase function, we wish to present five relevant facts concerning it. First, it is clear that the H and G parameters have been introduced with the aim to be two fundamental parameters to describe the photometric behavior of asteroids, or more generally, that of atmosphereless Solar-System bodies. On one hand, knowledge of these two parameters allows one to predict the magnitude expected for an object at any given phase angle. Conversely, fitting a given magnitude-phase data set using the H, G phase function allows one to directly obtain H (the absolute magnitude). However, Bowell et al. (1989) noted that the relation between size, albedo, and H, as given in Eq. (1), should be taken with a grain of salt. In particular, it was suggested that the albedo derived via H and size, being not a direct measurement, should be referred to as a "pseudoalbedo".

Second, the so-called phase integral[6] (q), is a linear function of G, viz.[7]:

$$q = 0.290 + 0.684G. \tag{7}$$

The importance of the phase integral q is that it is used to link the value of the geometric albedo to the value of the Bond albedo, which is by definition the ratio between the total flux of sunlight scattered (i.e., not absorbed) by an object and the incoming sunlight flux incident on the object. The simple relation between the geometric albedo p_V, Bond albedo A, and the phase integral q is the following:

$$A = p_V q. \tag{8}$$

Since the Bond albedo is an important parameter, for instance for studies of thermal infrared emission, the simple relation linking G to q is something generally useful.

Third, it is a fact that real objects have irregular shapes, and so exhibit a rotational modulation in their brightness. However, by definition, H refers to the average brightness during a rotational cycle. In practical terms, Bowell et al. (1989) noted that the phase function should be expected to work using magnitude values obtained at unknown rotational phases, although with greater uncertainty in the resultant parameters. In the future, when huge databases of sparse photometric data will be produced by surveys like Gaia and Pan-STARRS, modern techniques to invert sparse photometric data will, in principle, allow the rotational phase, at which each given observation was obtained, to be estimated (Cellino et al., 2007).

Fourth, there have been several analyses to find relations between G and some physical properties of asteroids. The results of these investigations (Tedesco, 1986; Harris and Young, 1989) indicate that there is a general trend of increasing G for increasing albedo. Taken at face value, these results indicate that the parameter G and albedo correlate but that this correlation is not particularly strong.

Finally, we note that it is inadvisable to combine magnitude data obtained at different apparitions (the interval of time around opposition during which an asteroid is observable) unless it has been established that the apparitions correspond to similar aspect angles, because different apparitions may correspond to different viewing geometries. In particular, the aspect angle may change from apparition to apparition, resulting in the object presenting different views of its surface to the observer. Thus, combining data from different apparitions can produce misleading results. In particular, the value of H for a given object may change from apparition to apparition. However, the consequences of this fact are beyond the scope of the present paper because it is something that is independent of the actual phase function.

2.2. Stochastic optimization

We make use of a stochastic optimization method for the basis functions that is, in principle, independent of any a priori analytical choices for the shape of the functions. We present the basis functions with a discretization and cubic-spline interpolation scheme relying on a fixed discrete set of phase angles, with the function values at the fixed angles and, occasionally, the first derivatives of the functions at the ends of the entire angular interpolation range as the free parameters (or unknowns). As a result, the number of free parameters is large but manageable. The optimization method includes ingredients from simulated annealing methods (e.g., Press et al., 1992; also compare to MCMC or Markov-Chain Monte-Carlo methods, Gilks et al., 1996). The optimization of the basis-function values proceeds from a chosen starting point via a Monte-Carlo method that proposes random moves based on Gaussian proposal probability densities, but gives rise to a move only if the proposed new point in the parameter space results in improved fits to all the observational data. The data are grouped according to differing phase-curve shapes to allow for wide applicability of the new basis functions. In optimizing the basis functions, the data are properly weighted by the asteroid groups and number of members within each group.

In the optimization, it is necessary to utilize regularization procedures to constrain the basis functions to be members of reasonable function classes. Among the typical constraints are, for example, that a basis function needs to be a monotonically decreasing function of the phase angle or that a basis function needs to have a positive second derivative close to the opposition to be able to describe common opposition-effect characteristics. The phase-angle discretization for cubic-spline interpolation needs to be defined so as to secure, preferably, numerous photometric observations of different asteroids within each of the discrete intervals. It is important to require that the basis functions be non-intersecting at phase angles most typically covered by observations: should the basis functions intersect, all resulting phase functions would pass through the point of intersection, which would be in disagreement with observational data. Furthermore, if the first derivatives of the basis functions coincide for some phase angle, the linear least-squares fitting becomes ill-posed in

[6] The phase integral is the integral of the phase function between 0° and 180°.
[7] Note that this H, G phase integral is numerically accurate to ~5%.

the vicinity of that phase angle. It is desirable to rule out this caveat, again, at phase angles most typically covered by observations.

The optimization scheme also works well for smaller numbers of parameters, i.e., when we optimize basis functions that use a small number of parameters (like the numerical coefficients of the basis functions in Eq. (6) for the approximate H, G phase function). In what follows, we utilize stochastic optimization methods in numerous tasks connected with the search for improved photometric phase functions.

Deriving the basis functions for the magnitude phase function entails solving a global optimization problem iteratively so that, at each iteration step, a number of linear least-squares minimization problems are solved for individual asteroid phase curves. We group the individual asteroid phase curves based on their similarities and differences so as to guarantee a balanced coverage of phase-curve variability.

The global metric to be minimized with respect to the N_P parameters $\boldsymbol{P} = (P_1, P_2, P_3, \ldots, P_{N_P})^T$ characterizing the basis functions is termed m^2:

$$m^2(\boldsymbol{P}) = \frac{1}{N}\sum_{i=1}^{N}\sum_{j=1}^{N_i}\sum_{k=1}^{N_{ij}}\frac{\left[V_{ijk} - V_{ij}(\alpha_{ijk}, \boldsymbol{P})\right]^2}{\sigma_{ijk}^2}, \tag{9}$$

where N is the number of asteroid groups involved, N_i is the number of asteroids in group i, N_{ij} is the number of observations of the jth asteroid in group i, V_{ijk} and α_{ijk} denote the kth observed magnitude and corresponding phase angle of asteroid j in group i, $V_{ij}(\alpha_{ijk}, \boldsymbol{P})$ is the computed magnitude, and σ_{ijk}^{-2} denotes the weight factor for each observation.

The computed magnitudes $V_{ij}(\alpha_{ijk}, \boldsymbol{P})$ in Eq. (9) follow from solving the linear least-squares problems concerning the observed disk-integrated brightnesses L_{ijk}, their error standard deviations $\sigma_{ijk}^{(L)}$, and the computed disk-integrated brightnesses $L_{ij}(\alpha_{ijk}, \boldsymbol{a}_{ij})$, where $\boldsymbol{a}_{ij} = (a_{1,ij}, a_{2,ij}, \ldots, a_{N_a,ij})^T$ denotes the N_a parameters to be fitted in the linear least-squares sense for each asteroid ij. We have the interrelations

$$\begin{aligned} L_{ijk} &= 10^{-0.4V_{ijk}}, \\ \sigma_{ijk}^{(L)} &= L_{ijk}\left(10^{0.4\sigma_{ijk}^{(V)}} - 1\right), \end{aligned} \tag{10}$$

where $\sigma_{ijk}^{(V)}$ stands for the error standard deviations of the magnitudes. The χ^2-value to be minimized here with respect to the parameters $\boldsymbol{a}_{ij}$ is

$$\chi_{ij}^2(\boldsymbol{a}_{ij}) = \sum_{k=1}^{N_{ij}}\frac{\left[L_{ijk} - L_{ij}(\alpha_{ijk}, \boldsymbol{a}_{ij})\right]^2}{\left[\sigma_{ijk}^{(L)}\right]^2}. \tag{11}$$

The computed disk-integrated brightnesses are expressed with the help of the N_a basis functions $\Phi_1(\alpha, \boldsymbol{P}), \Phi_2(\alpha, \boldsymbol{P}), \ldots, \Phi_{N_a}(\alpha, \boldsymbol{P})$,

$$\begin{aligned} L_{ij}(\alpha_{ijk}, \boldsymbol{a}_{ij}) &= \sum_{l=1}^{N_a} a_{ijl}\Phi_l(\alpha_{ijk}, \boldsymbol{P}), \\ \Phi_l(0, \boldsymbol{P}) &= 1, \quad l = 1, 2, \ldots, N_a. \end{aligned} \tag{12}$$

The minimization gives us $\boldsymbol{a}_{ij,\mathrm{ls}}$, the linear least-squares $\boldsymbol{a}_{ij}$, for a given set of basis functions parameterized by $\boldsymbol{P}$. The magnitudes are then computed from

$$V_{ij}(\alpha_{ijk}, \boldsymbol{P}) = -2.5\log_{10}L_{ij}(\alpha_{ijk}, \boldsymbol{a}_{ij,\mathrm{ls}}). \tag{13}$$

The metric $m^2(\boldsymbol{P})$ now follows from Eq. (9). The steps in Eqs. (9)–(13) are iteratively repeated for varying $\boldsymbol{P}$ until convergence on the minimum $m^2(\boldsymbol{P})$-metric parameters $\boldsymbol{P} = \boldsymbol{P}_{\mathrm{ls}}$ is achieved. Note that individual asteroid brightnesses are being fitted in the linear least-squares sense, whereas the computation of $m^2(\boldsymbol{P})$ entails the least-squares solution in terms of magnitudes. We have verified that the least-squares parameters $\boldsymbol{P}_{\mathrm{ls}}$ are not sensitive to whether magnitudes or brightnesses are utilized in the definition of $m^2(\boldsymbol{P})$.

The weight factors σ_{ijk}^{-2} in Eq. (9) describe the weight of each asteroid observation in the global m^2-metric. The weight factors depend on the number of asteroids in each group N_i and $\sigma_{ijk}^{(V)}$ as follows:

$$\begin{aligned} \sigma_{ijk}^2 &= \frac{\left[\sigma_{ijk}^{(V)}\right]^2}{w_i}, \\ w_i &= \left[\sum_{j=1}^{N_i}\sum_{k=1}^{N_{ij}}\frac{1}{\left[\sigma_{ijk}^{(V)}\right]^2}\right]^{-1}. \end{aligned} \tag{14}$$

The weight factor w_i ensures that each asteroid group i obtains the same weight in the global optimization, without regard to the number or accuracy of the observations. Within individual data sets and within each group, accurate observations obtain more weight than inaccurate ones.

The global χ^2-value corresponding to the m^2-metric of Eq. (9) is available from

$$\chi^2(\boldsymbol{P}) = Nm^2(\boldsymbol{P})\left[\sum_{i=1}^{N} w_i\right]^{-1}. \tag{15}$$

In what follows, we nevertheless characterize the goodness of each basis-function set by the global m-metric value (in mag) following from the square root of the m^2-metric in Eq. (9). In characterizing the goodness of the linear least-squares fits for the individual brightness phase curves, we make use of the rms-values of the fits (in mag, again).

Note that the m-metric could, in principle, include terms measuring the predictive power of the magnitude phase function, as well as terms measuring the errors in the parameters $\boldsymbol{a}$ (omitting the subscripts ij). In the present work, we are making use of the m-metric as given in Eq. (9).

2.3. Monte-Carlo inverse methods

For a given magnitude phase function, the a posteriori probability density function (p.d.f.) for the parameters $\boldsymbol{a}$ is obtained from (cf. Eq. (11))

$$p(\boldsymbol{a}) \propto \exp\left[-\frac{1}{2}\chi^2(\boldsymbol{a})\right], \tag{16}$$

where χ^2 denotes the product of the residuals in a row vector (observed minus computed), the covariance matrix for the random observational errors, and the residuals in a column vector. In what follows, for simplicity, the covariance matrix is assumed to be diagonal. If the model is linear, $p(\boldsymbol{a})$ is a multivariate Gaussian p.d.f. and can be Monte-Carlo sampled using standard methods, whereafter samples of dependent nonlinear parameters follow in a straightforward way.

For a model with one nonlinear parameter (b) and a number of linear parameters ($\boldsymbol{a}$), we obtain varying multivariate Gaussian p.d.f.s for $\boldsymbol{a}$ given the value of b. Furthermore, the marginal p.d.f. of b is

$$p(b) \propto \sqrt{\det\Sigma_{\boldsymbol{a}}(b)}\exp\left[-\frac{1}{2}\chi_{\boldsymbol{a}}^2(b)\right], \tag{17}$$

where $\Sigma_{\boldsymbol{a}}(b)$ and $\chi_{\boldsymbol{a}}^2(b)$ denote the covariance matrix and value of χ^2 due to the least-squares solution for $\boldsymbol{a}$ given the value of b. The a posteriori p.d.f. in Eq. (17) can be efficiently sampled by drawing b from its marginal p.d.f. and then drawing $\boldsymbol{a}$ from the multivariate Gaussian p.d.f. corresponding to the value of b sampled.

Table 1
Asteroid groups I and II utilized in the development of the magnitude phase functions. We show the V-band geometric albedo p_V (Tedesco et al., 2002a), the number of observations N_{obs}, the minimum and maximum phase angles of the observations α_{min} and α_{max}, and the references to the observations.

Group	Asteroid	Class	p_V	N_{obs}	α_{min}	α_{max}	References
I	(50) Virginia	X, Ch	0.04	18	0.15	23.1	Shevchenko et al. (1997)
	(59) Elpis	CP, B	0.04	15	0.30	21.1	Shevchenko et al. (1996)
	(102) Miriam	P, C	0.05	11	0.11	23.7	Shevchenko et al. (1997)
	(190) Ismene	P		14	0.30	14.9	Shevchenko et al. (2008)
	(1021) Flammario	F, B	0.05	7	0.20	12.9	Belskaya et al. (in preparation)
II	(10) Hygiea	C	0.07	17	0.32	17.1	Shevchenko (1997)
	(24) Themis	C, B	0.08	22	0.34	20.8	Harris et al. (1989a)
	(47) Aglaja	C, B	0.08	25	0.10	11.2	Chernova et al. (1991)
	(303) Josephina	C	0.06	16	0.17	17.8	Shevchenko et al. (2008)

Table 2
As in Table 1 for groups III–V except for (2867) Steins, for which simulated data is being utilized.

Group	Asteroid	Class	p_V	N_{obs}	α_{min}	α_{max}	References
III	(5) Astraea	S	0.23	7	0.33	15.7	Shevchenko et al. (2002)
	(6) Hebe	S	0.27	11	1.3	22.9	Gehrels and Taylor (1977)
	(20) Massalia	S	0.21	16	0.09	27.4	Gehrels (1956) and Belskaya et al. (2003)
	(79) Eurynome	S	0.26	12	0.07	29.2	Shevchenko et al. (1996)
IV	(44) Nysa	E	0.54	23	0.17	21.5	Harris et al. (1989b)
	(64) Angelina	E	0.48	11	0.11	22.5	Harris et al. (1989b)
V	(1862) Apollo	Q	0.26	18	0.2	89.0	Harris et al. (1987)
	The Moon	–	0.17	17	0.5	140.0	Bowell et al. (1989)
	Deimos	–	0.07	15	1.0	120.0	Pang et al. (1983)

We choose to characterize the parameter errors using the 3σ (99.7%) and 1σ (68.3%) criteria in the following way: from the set of sampled parameters, we determine the $\chi^2(\boldsymbol{a})$-value corresponding to the 99.7% or 68.3% boundaries, whereafter we give the two-sided error bars of the parameters corresponding to the minimum and maximum values of the parameters within the 99.7% or 68.3% set of sampled parameters.

3. Results and discussion

3.1. Optimizing the H, G phase function

Our first attempt to obtain an improvement of the H, G phase function consists of trying to derive improved expressions for the basis functions $\Phi_1(\alpha)$ and $\Phi_2(\alpha)$. The shapes of the phase curves observed for E-class and F-class asteroids are such that the phase curves intersect each other at a small but nonzero phase angle when normalized to an equal magnitude value at zero phase angle (see references in Tables 1 and 2). Thus, a linear two-parameter phase function with non-intersecting basis functions cannot result in excellent fits to the entire current asteroid phase-curve data. In what follows, we assess in detail the price of having such a phase function.

The data used in this analysis are summarized in Tables 1 and 2, which also list the original references for each phase curve. We selected what we believe to be the best data available today, in terms of good phase-angle coverage at small phase angles, good phase-angle range, and small scatter within the observational data (typically $\lesssim$0.03 mag). In particular, we used a total of 18 phase curves, subdivided into five groups I–V. Four of the groups (I–IV) were established because of similar photometric behavior of the objects. Differences between the phase curves of individual asteroids in each of these groups are within the uncertainties of the magnitude measurements, and the data are utilized to produce four composite phase curves pertaining to groups I–IV. These four groups are mainly characterized by differences in geometric albedo, but we did not do any a priori selection based on albedo and/or taxonomic class, but rather focused on the apparent photometric behavior by looking at the data on a case-by-case basis. In simple terms, the four groups include asteroids which exhibit increasing extents of the opposition brightness surge, from objects displaying mostly linear phase curves with very little opposition effect, if any, up to objects displaying a pronounced opposition effect (the latter objects belonging to the E taxonomic class).

The remaining group V consists of photometry for four objects with phase-curve observations extending over extensive ranges of phase angles: (1862) Apollo, the Moon, (2867) Steins, and the martian moon Deimos. Note that the phase curve of Asteroid (2867) Steins is simulated using the H, G phase function with $G \approx 0.4$ in five-degree steps from $\alpha = 0°$ to $\alpha = 150°$ (with the standard deviation $\sigma^{(V)}$ taken to be $\sim$0.02 mag). The simulation relies on the space-based ESA Rosetta observations (Sonia Fornasier, private communication 2009). Tables 1 and 2 show that the high-quality phase curves obtained in recent years have been mostly produced by V. Shevchenko at the Kharkiv Observatory.

In summary, groups I–V contribute altogether eight different phase curves to the optimization process. Making the composite curves for groups I–IV is presently required in order to obtain a coverage as a function of the phase angle dense enough for

Table 3
The basis functions Φ_1 and Φ_2 of the H, G_1, G_2 magnitude phase function. Values at intermediate phase angles follow from cubic splines passing through the tabulated points with the requirement that the first derivatives are $\Phi_1'\left(\frac{\pi}{24}\right) = -\frac{6}{\pi}$, $\Phi_2'\left(\frac{\pi}{24}\right) = -\frac{9}{5\pi}$, $\Phi_1'\left(\frac{5\pi}{6}\right) = -9.1328612 \times 10^{-2}$, and $\Phi_2'\left(\frac{5\pi}{6}\right) = -8.6573138 \times 10^{-8}$. We give the numerical values with high precision to allow for sufficient accuracy when utilized in the cubic-spline analyses. For the basis function Φ_3, see Table 4.

α (°)	Φ_1	Φ_2
7.5	7.5×10^{-1}	9.25×10^{-1}
30.0	3.3486016×10^{-1}	6.2884169×10^{-1}
60.0	1.3410560×10^{-1}	3.1755495×10^{-1}
90.0	5.1104756×10^{-2}	1.2716367×10^{-1}
120.0	2.1465687×10^{-2}	2.2373903×10^{-2}
150.0	3.6396989×10^{-3}	1.6505689×10^{-4}

Table 4
The basis function Φ_3 of the H, G_1, G_2 phase function. Values at intermediate phase angles follow from cubic splines passing through the tabulated points with the requirement that the first derivatives are $\Phi_3'(0) = -1.0630097 \times 10^{-1}$ and $\Phi_3'(\frac{\pi}{6}) = 0$.

α (°)	Φ_3
0.0	1
0.3	8.3381185×10^{-1}
1.0	5.7735424×10^{-1}
2.0	4.2144772×10^{-1}
4.0	2.3174230×10^{-1}
8.0	1.0348178×10^{-1}
12.0	6.1733473×10^{-2}
20.0	1.6107006×10^{-2}
30.0	0

Table 5
Additional objects utilized in the illustration of the new magnitude phase function. We show the V-band geometric albedo p_V (Tedesco et al., 2002a), the number of observations N_{obs}, the minimum and maximum phase angles of the observations α_{min} and α_{max}, and the references to the observations. For (24) Themis, (44) Nysa, (1862) Apollo, and the Moon, see Tables 1 and 2.

Asteroid	Class	p_V	N_{obs}	α_{min}	α_{max}	References
(69) Hesperia	M	0.14	21	0.13	16.0	Poutanen et al. (1985)
(82) Alkmene	S	0.21	11	2.29	27.2	Harris et al. (1984b)
(133) Cyrene	SR	0.26	11	0.20	13.2	Harris et al. (1984a)
(419) Aurelia	F	0.05	7	0.62	15.4	Harris and Young (1988)

successful optimization of basis functions. Following the notation in Section 2, we have $N = 5$, $N_i = 1$ for $i = 1$–4, and $N_5 = 4$. The standard deviation $\sigma^{(V)}$ (subscripts suppressed) of Section 2.2 obtains the value of 0.03 mag for all objects except the Moon (0.023 mag, Bowell et al., 1989) and (2867) Steins (0.023 mag). For observations at large phase angles $\alpha \geqslant 100°$, we assume $\sigma^{(V)} = 0.2$ mag mainly due to the relevance of unmodeled physical properties of the objects such as the irregular shape and variegation of scattering properties on the surfaces. For observations at small phase angles $\alpha \leqslant 0.2°$ for members in groups I–IV, we halve the $\sigma^{(V)}$-value in order for the resulting phase functions to be able to produce particularly accurate fits at small phase angles.

In attempting to revise the two H, G basis functions, we follow two principal approaches: first, by discretizing the basis functions and introducing a fixed cubic-spline interpolation grid of phase angles (0°, 0.3°, 1°, 2°, 4°, 8°, 15°, 30°, 60°, 90°, 120°, and 150°), we search for function values resulting in minimum global m^2 in Eq. (9); second, we fine-tune the numerical coefficients of the current H, G basis functions in Eq. (6). In both approaches, we require

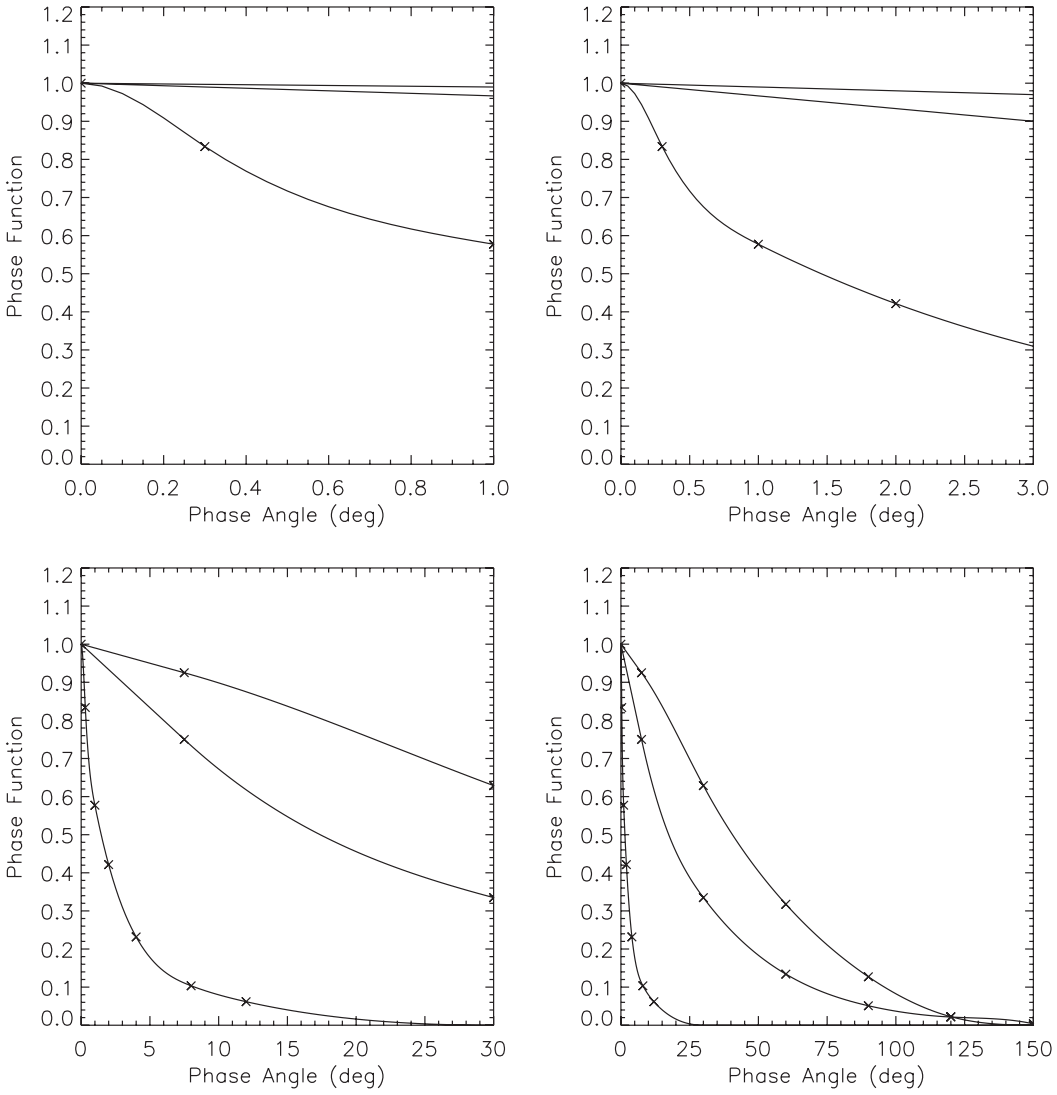

Fig. 1. The basis functions of the three-parameter H, G_1, G_2 magnitude phase function expressed using cubic splines (Tables 3 and 4).

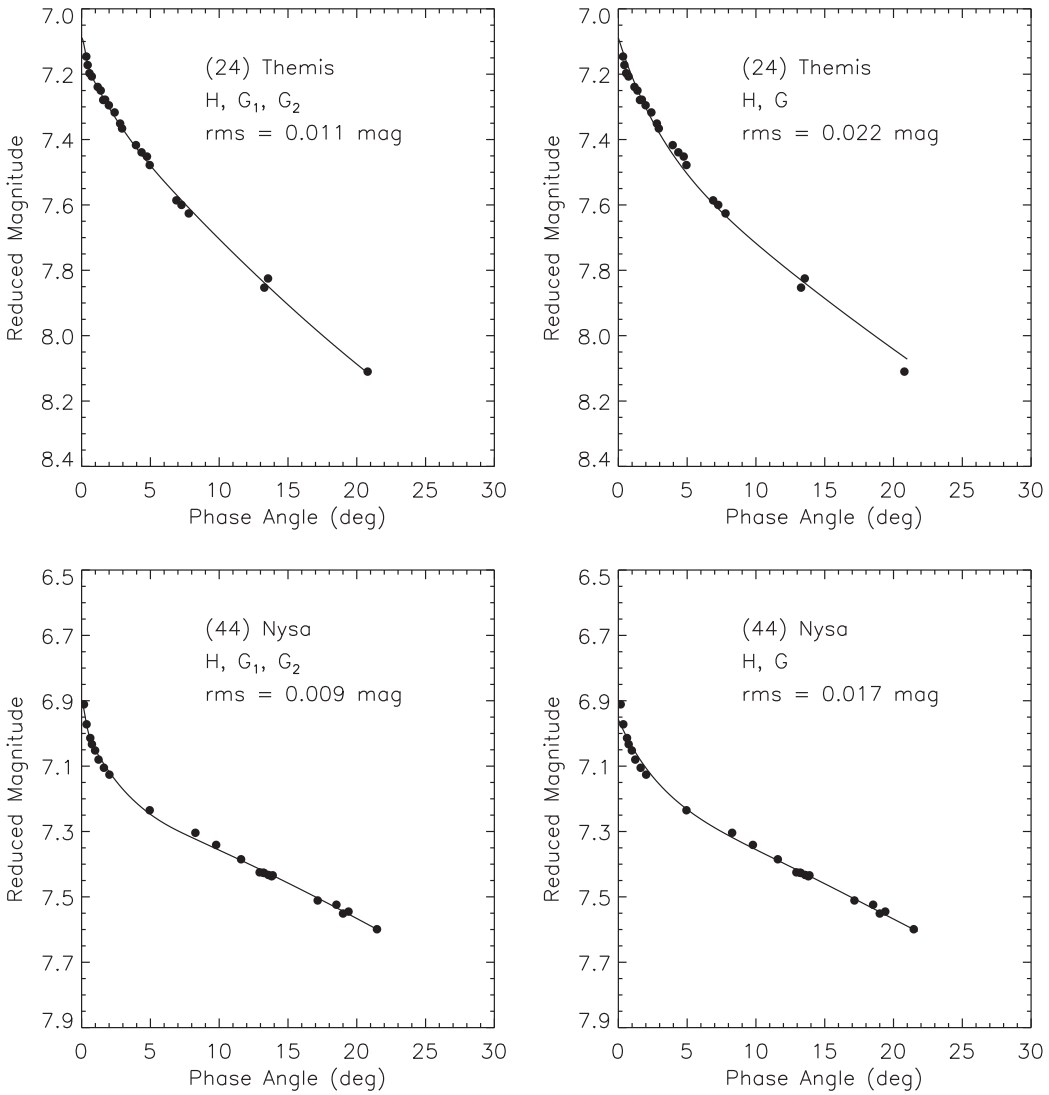

Fig. 2. Linear least-squares fits (solid lines) to the phase curves of the C-class Asteroid (24) Themis (top) and the E-class Asteroid (44) Nysa (bottom) using the H, G_1, G_2 (left) and H, G magnitude phase functions (right). For best-fit parameters and their error estimates, see Table 6.

that $0 \leqslant G \leqslant 1$. Before revising the basis functions, we note that the H, G phase function fits the data set with $m = 0.0361$ mag.

Within the first approach, first, we further require that the two basis functions do not intersect at phase angles $\alpha > 0°$. Second, we require that the values of the basis functions at the discretization points be monotonically decreasing across the full phase-angle range; and, third, we require that the approximate second derivative of the first basis function (when computed using finite differences at the discretization points) is positive everywhere and that the second derivative of the second basis function is positive for $\alpha > 8°$. Applying these constraints and carrying out the stochastic optimization procedure results in a phase function for which $m = 0.0304$ mag, that is, we have removed about one third of the original m^2-value for the H, G phase function. However, strong trends in the residuals are present at large phase angles and the basis functions are by no means simple.

Within the second approach, as above, we do not allow the basis functions to intersect. We do not incorporate additional constraints and obtain $m = 0.0351$ mag with new numerical coefficients to replace those in Eq. (6). This shows only minute improvement compared to the fit using the H, G phase function and shows that the H, G phase function has been well optimized. The main conclusions are similar to those of the first approach. Note that all the m-values being close to the typical observational error standard deviation of 0.03 mag shows that, overall, the phase functions fit the observational data reasonably well.

We do not include any figures showing the results of our attempt at simply improving the H, G phase function because the fits that we obtained were sometimes significantly better but sometimes worse than the corresponding H, G fits and because many cases of fits using the H, G phase function will be displayed in the figures presented in Section 3.3.

The results of this first exercise are thus negative concerning the development of a linear two-parameter phase function. In particular, we do not find a way to reach precise fits to the best data currently available. We are forced to conclude that any "improved" linear two-parameter phase function using fixed basis functions has serious problems in adequately fitting a number of very accurate magnitude phase curves.

On the basis of these results, we conclude that no "minor" revision of the H, G phase function will lead to a substantial improvement of the best fit to high-quality photometric phase data. This is essentially due to the intrinsic limits imposed by the adoption of a

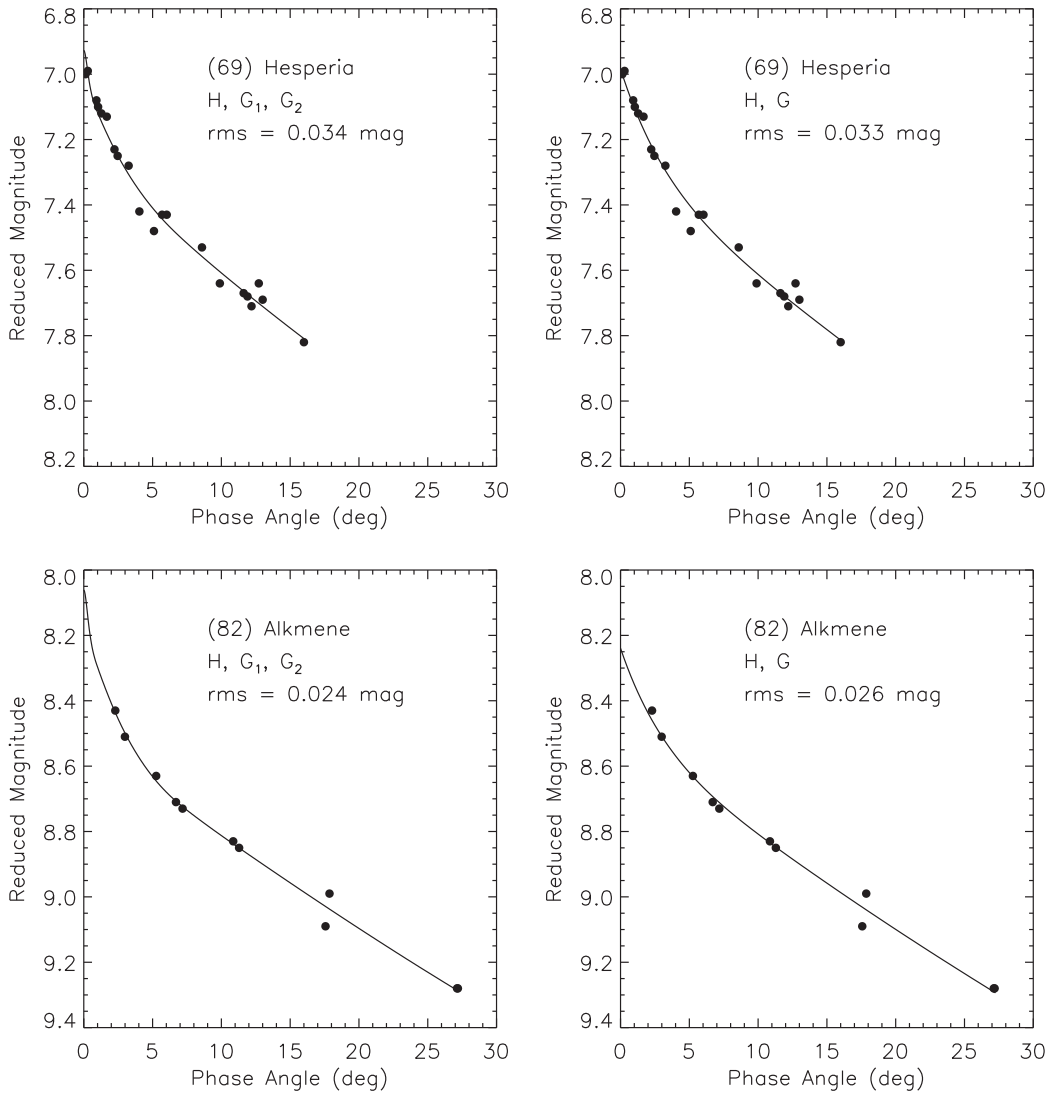

Fig. 3. As in Fig. 2 for the M-class Asteroid (69) Hesperia and the S-class Asteroid (82) Alkmene.

linear two-parameter phase function. Although this kind of model has the merit of being very simple, a better fit of high-quality photometric phase data can only be obtained by adding an additional parameter to the photometric phase function.

3.2. H, G_1, G_2 phase function

An immediate critical comment on the conclusion above is that adding parameters necessarily leads to better fits (e.g., by using $N_a > 3$ free parameters one expects to get even better fits), therefore the reasons for adding even one single parameter must be compelling and well justified. In what follows, we assess the feasibility of a three-parameter magnitude phase function that, in the number of free parameters, represents the minimum change to the two-parameter H, G phase function.

In a three-parameter H, G_1, G_2 magnitude phase function for asteroids, the reduced observed magnitudes $V(\alpha)$ can be obtained from

$$\begin{aligned} 10^{-0.4V(\alpha)} &= a_1\Phi_1(\alpha) + a_2\Phi_2(\alpha) + a_3\Phi_3(\alpha) \\ &= 10^{-0.4H}[G_1\Phi_1(\alpha) + G_2\Phi_2(\alpha) + (1 - G_1 - G_2)\Phi_3(\alpha)], \end{aligned} \quad (18)$$

where $\Phi_1(0) = \Phi_2(0) = \Phi_3(0) = 1$. The absolute magnitude H and the coefficients G_1 and G_2 are

$$\begin{aligned} H &= -2.5\log_{10}(a_1 + a_2 + a_3), \\ G_1 &= \frac{a_1}{a_1 + a_2 + a_3}, \\ G_2 &= \frac{a_2}{a_1 + a_2 + a_3}. \end{aligned} \quad (19)$$

The coefficients a_1, a_2, and a_3 are estimated from the observations by using the linear least-squares method. Thereafter, H, G_1, and G_2 follow from the nonlinear relations in Eq. (19).

The next goal is to determine the basis functions $\Phi_1(\alpha)$, $\Phi_2(\alpha)$, and $\Phi_3(\alpha)$. We start by searching for a magnitude phase function where there is a single opposition-effect function and where there is a possibility for obtaining arbitrary quasi-linear slopes of the phase functions at larger phase angles. Thus, we construct a magnitude phase function consisting of an opposition-effect function Φ_3 and two linear basis functions Φ_1 and Φ_2, and study such a phase function for $\alpha < 30°$. Accordingly, the basis functions Φ_1 and Φ_2 are taken to be

$$\begin{aligned} \Phi_1(\alpha) &= 1 - \frac{6\alpha}{\pi}, \\ \Phi_2(\alpha) &= 1 - \frac{9\alpha}{5\pi}, \end{aligned} \quad (20)$$

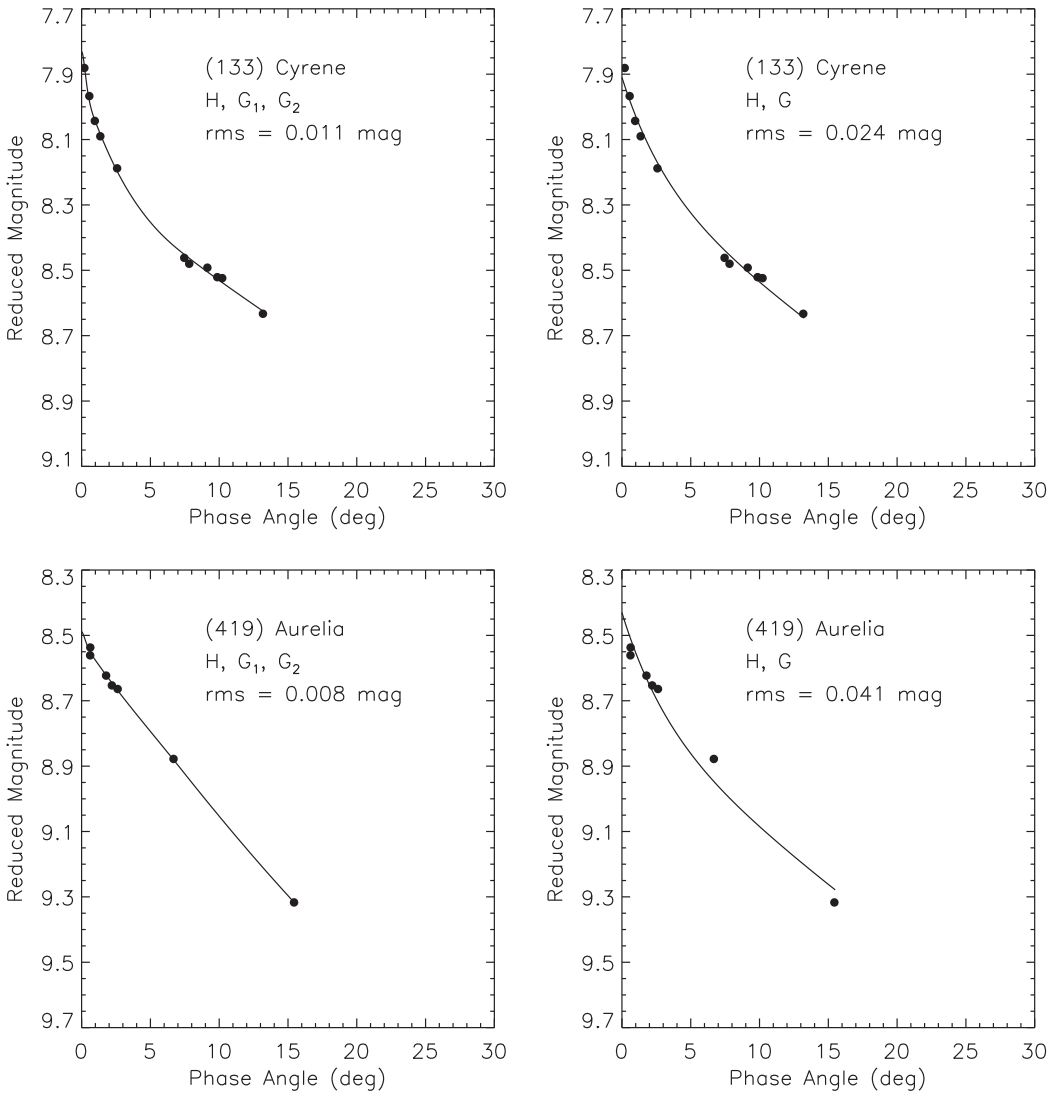

Fig. 4. As in Fig. 2 for the SR-class Asteroid (133) Cyrene and the F-class Asteroid (419) Aurelia.

bracketing the photometric slopes currently observed for asteroids and partly mimicking the H, G basis functions. Note that $\Phi_1(\frac{\pi}{6}) = 0$ and $\Phi_2(\frac{\pi}{6}) = \frac{7}{10}$.

We search for Φ_3 by using the stochastic optimization method of Section 2.2 applied to the observational data in the five groups described above at $\alpha \leqslant 30°$. First, by assuming that Φ_3 is of the same functional form as the approximate H, G basis functions (Eq. (6)), the stochastic optimization suggests

$$\Phi_3(\alpha) = \exp\left(-4\pi \tan^{\frac{2}{3}}\frac{1}{2}\alpha\right) \tag{21}$$

with $m = 0.0230$ mag. For the two numerical coefficients, having in mind realistic amplitudes for the opposition effect, we have adopted 4π and $\frac{2}{3}$. We point out, however, that there turns out to be an infinite number of other suitable pairs of coefficients that also allow for satisfactory phase-curve fits. Second, by using cubic splines for $\Phi_3(\alpha)$, we obtain fits with $m = 0.0213$ mag indicating further improvement.

We can now search for the general H, G_1, G_2 phase function valid across $0° \leqslant \alpha \leqslant 150°$ and thus the full phase-angle range covered by the observations, that is, $0° \leqslant \alpha \leqslant 140°$ (for the phase-angle grids, see Tables 3 and 4). For the derivation of the H, G_1, G_2 phase function, we recall that $N = 5$ with $N_1 = N_2 = N_3 = N_4 = 1$ and $N_5 = 4$.

As a starting point for stochastic optimization, we assume Φ_1 and Φ_2 equal to the linear dependences in Eq. (20) for $\alpha \leqslant 7.5°$ and equal to the H, G basis functions for $\alpha > 7.5°$, respectively, and assume Φ_3 based on Eq. (21). We stress that this starting point does not result in acceptable fits to the observations but only serves to initiate the optimization successfully with three non-intersecting basis functions within $\alpha \lesssim 120°$. In the optimization, we do not vary the linear parts of Φ_1 and Φ_2 within $\alpha \leqslant 7.5°$. For the spline parts of Φ_1 and Φ_2, the first derivatives at $\alpha = 7.5°$ are then fixed according to the linear dependences, whereas the first derivatives at $\alpha = 150°$ are treated as free parameters constrained to have negative values. In optimizing Φ_3 using splines, it is assumed that $\Phi_3(\alpha \geqslant \frac{\pi}{6}) = 0$ and $\Phi_3'(\frac{\pi}{6}) = 0$, whereas the first derivative at $\alpha = 0°$ is treated as a free parameter with a negative value. To summarize, the number of free basis-function parameters is $N_P = 20$.

After optimization, the m-metric reaches the value of $m = 0.0188$ mag that is clearly the best value for the m-metric of all the phase functions presently assessed and is even smaller than the nominal observational errors assumed. Note that the H, G_1, G_2 phase function works over the full phase-angle range of 0–140° covered by the observations. In particular, the phase function nicely fits the small-phase-angle observations of E-class asteroids.

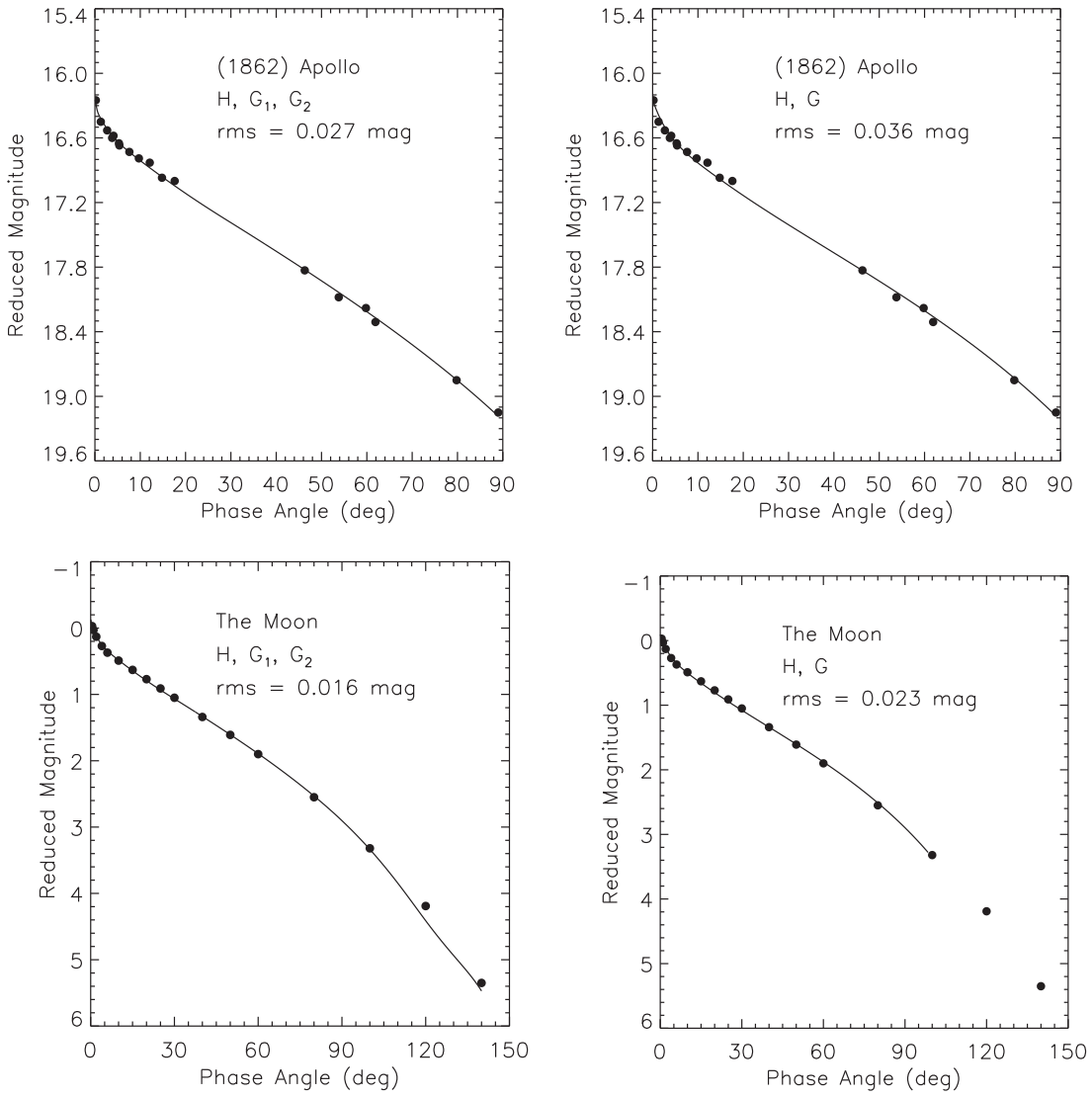

Fig. 5. As in Fig. 2 for the Q-class near-Earth object (1862) Apollo and for the Moon. For the latter, the rms-values describe the residuals for 0–100° in phase angle.

It is nevertheless plausible that the H, G_1, G_2 phase function will need to be improved once more observational data become available at large phase angles.

The basis functions of the H, G_1, G_2 phase function following from the optimization are depicted in Fig. 1 and given explicitly in Tables 3 and 4. There are three additional dependent parameters of interest in applications of the H, G_1, G_2 phase function. First, the phase integral is written as a function of G_1 and G_2 as

$$q = 0.009082 + 0.4061G_1 + 0.8092G_2. \tag{22}$$

Second, we introduce a photometric phase coefficient k defined as follows:

$$k = -\frac{G_1\frac{6}{\pi} + G_2\frac{9}{5\pi}}{G_1 + G_2} = -\frac{1}{5\pi}\frac{30G_1 + 9G_2}{G_1 + G_2}. \tag{23}$$

Thus, k is the normalized slope of the phase-curve part represented by Φ_1 and Φ_2 for $\alpha \leqslant 7.5°$. Third, we introduce the amplitude of the opposition effect $\zeta - 1$, where ζ is the so-called enhancement factor:

$$\zeta - 1 = \frac{1 - G_1 - G_2}{G_1 + G_2}. \tag{24}$$

3.3. Application of the H, G_1, G_2 phase function

In order to illustrate how well the new H, G_1, G_2 magnitude phase function manages to describe phase curves, we utilize the observational data in Bowell et al. (1989). We thus fit the phase curves of (24) Themis, (44) Nysa, (69) Hesperia, (82) Alkmene, (133) Cyrene, (419) Aurelia, (1862) Apollo, and the Moon by using the H, G phase function (with the precise basis functions in Eq. (5)) and the new H, G_1, G_2 phase function.[8] The data are described briefly in Tables 5, 1, and 2 with references to the original observations.

Figs. 2–5 show the least-squares fits to the observations in detail, allowing for a comparison between the fits using the H, G and H, G_1, G_2 phase functions. Table 6 gives the parameters with 99.7% error estimates. We do not give the corresponding numbers as resulting from the original H, G magnitude system, as the official H, G error analysis differs from the analyses presently adopted (Section 2.3). In the figures, we have chosen to give the best-fit curves only, in order to allow easy comparison of the curves resulting from different phase functions. The 99.7% error envelopes are

[8] Note that Bowell et al. (1989) did not provide figures for H, G fits.

Table 6
The H, G_1, G_2 magnitude phase function as fitted to the photometric observations of asteroids and the Moon: the absolute magnitude H, coefficients G_1 and G_2, phase integral q, opposition-effect amplitude $\zeta - 1$, and the photometric slope k, all with two-sided 99.7% (or 3σ) errors. On the final row, we give the rms-values of the individual fits. For the Moon, the rms-value describes the residuals for 0–100° in phase angle.

	(24) Themis	(44) Nysa	(69) Hesperia	(82) Alkmene	(133) Cyrene	(419) Aurelia	(1862) Apollo	Moon
H (mag)	7.063	6.929	6.940	8.00	7.853	8.47	16.260	−0.154
	−0.048	−0.095	−0.083	−0.19	−0.110	−0.12	−0.108	−0.057
	+0.104	+0.054	+0.055	+0.39	+0.076	+0.18	+0.089	+0.118
G_1	0.62	0.050	0.36	0.17	0.21	0.95	0.38	0.36
	−0.24	−0.259	−0.25	−0.28	−0.45	−0.54	−0.12	−0.12
	+0.28	+0.269	+0.28	+0.46	+0.52	+0.69	+0.15	+0.14
G_2	0.14	0.67	0.29	0.39	0.39	−0.057	0.354	0.338
	−0.16	−0.15	−0.18	−0.13	−0.33	−0.399	−0.051	−0.052
	+0.16	+0.14	+0.16	+0.11	+0.30	+0.318	+0.052	+0.049
q	0.379	0.573	0.393	0.395	0.411	0.348	0.451	0.429
	−0.040	−0.037	−0.041	−0.070	−0.079	−0.072	−0.041	−0.035
	+0.043	+0.040	+0.042	+0.122	+0.075	+0.073	+0.048	+0.038
$\zeta - 1$	0.30	0.39	0.53	0.79	0.66	0.12	0.36	0.43
	−0.19	−0.24	−0.21	−0.69	−0.40	−0.30	−0.19	−0.20
	+0.21	+0.30	+0.29	+1.06	+0.61	+0.42	+0.21	+0.21
k (°)$^{-1}$	−0.0289	−0.0116	−0.0229	−0.0170	−0.018	−0.0348	−0.0221	−0.0220
	−0.0049	−0.0071	−0.0069	−0.0091	−0.013	−0.0078	−0.0024	−0.0026
	+0.0058	+0.0097	+0.0082	+0.0138	+0.021	+0.0103	+0.0028	+0.0030
rms (mag)	0.011	0.009	0.034	0.024	0.011	0.008	0.027	0.016

available upon request. Note, however, that the tabulated error estimates for H partly characterize the extents of the envelopes.

We conclude that reasonable accuracies follow for the absolute magnitudes H, phase integrals q, and photometric slopes k; whereas, for the G_1 and G_2 parameters and the opposition-effect amplitude $\zeta - 1$, the errors are typically large. For (1862) Apollo and the Moon, we obtain G_1 and G_2 with improved accuracies. In this context, it is worth emphasizing that the parameter error estimates are to be interpreted by bearing in mind the purely empirical character of the phase functions.

(24) Themis. Both phase functions yield acceptable fits to the phase curve of (24) Themis, but it is notable that the H, G_1, G_2 phase function is capable of removing about half of the rms-value for the H, G fit.

(44) Nysa. Based on the rms-values only, both phase functions again yield acceptable fits. However, the H, G phase function fails to reproduce the sharpness of the opposition effect at the smallest phase angles.

(69) Hesperia. The H, G phase function provides a better fit to the phase curve of (69) Hesperia. Note that there is particularly strong fluctuation in the photometric observations of this asteroid which may explain the slightly larger rms-value for the H, G_1, G_2 fit.

(82) Alkmene. The two least-squares fits are almost equally good for (82) Alkmene, but there are clear differences close to the zero phase angle, where the H, G_1, G_2 phase function suggests an opposition effect stronger than that from the H, G phase function. According to Table 6, the H-value resulting from the H, G_1, G_2 phase function has rather large error bars, thus nicely allowing for more realistic less pronounced opposition effects.

(133) Cyrene. The H, G_1, G_2 phase function produces an excellent fit to the phase-curve data of (133) Cyrene, whereas the H, G phase function faces challenges at small phase angles.

(419) Aurelia. The H, G phase function fails to reproduce the quasi-linear phase-angle dependence for (419) Aurelia, whereas the H, G_1, G_2 phase function produces an excellent fit. The rms-value for the H, G_1, G_2 fit is less than a quarter of the one for the H, G fit.

(1862) Apollo. The H, G_1, G_2 phase function reproduces the full phase curve of (1862) Apollo accurately, whereas fitting the H, G phase function appears to result in systematic residual trends at small phase angles.

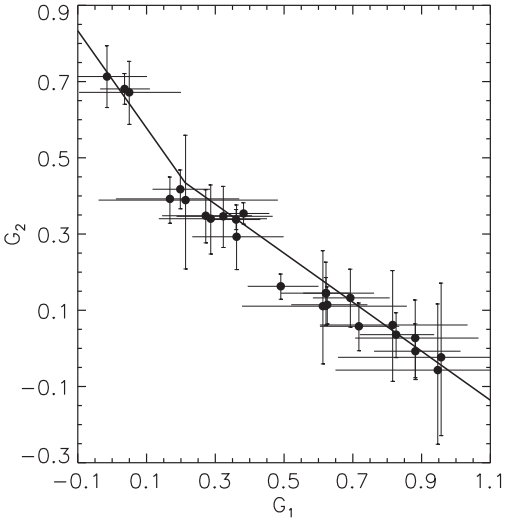

Fig. 6. The G_1 and G_2 parameters with 68.3% error domains for all objects presently studied (Tables 1, 2, and 5).

Moon. The H, G_1, G_2 phase function fits the lunar phase curve for $\alpha \in [0.5°, 100°]$ accurately and provides a reasonable description of the phase curve for $\alpha \geqslant 100°$. The H, G phase function provides a satisfactory fit to the phase curve for $\alpha \in [0.5°, 100°]$.

Note that the phase curves of (24) Themis, (44) Nysa, (1862) Apollo, and the Moon have been included in the derivation of the new magnitude phase function, which partly explains the remarkably small rms-values for the H, G_1, G_2 fits for these objects. Recall that, for large phase angles, there are observations of the martian moon Deimos, the Moon, Asteroid (1862) Apollo, as well as the simulated observations of (2867) Steins that have been utilized in developing the new phase function.

Fig. 6 depicts the G_2 parameter versus the G_1 parameter with 68.3% error domains for all objects presently studied using the H, G_1, G_2 magnitude phase function. The scatter plot can be seen to consist of three clusters that correspond to the objects with steep

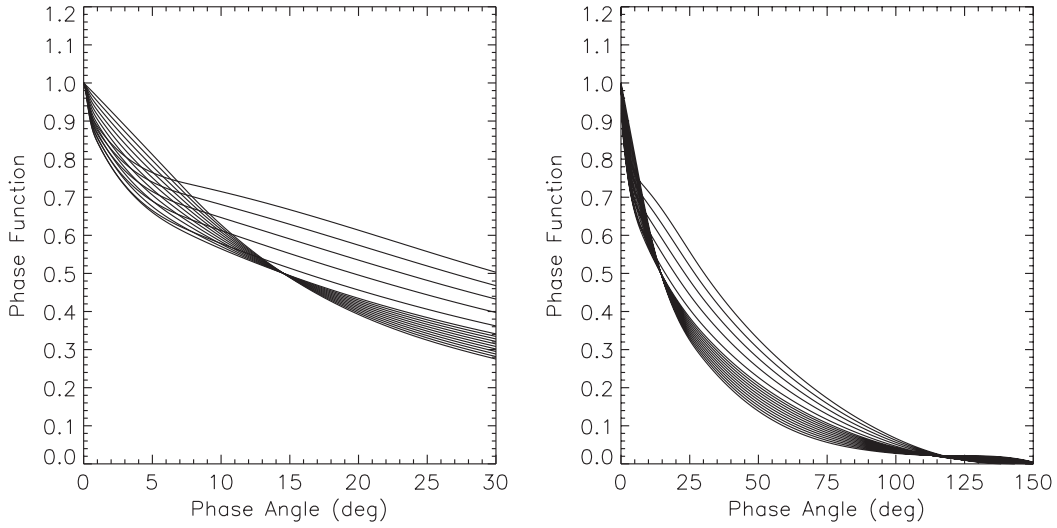

Fig. 7. The spectrum of phase-function shapes resulting from the nonlinear two-parameter H, G_{12} magnitude phase function.

Table 7
The H, G_{12} magnitude phase function as fitted to the photometric observations of asteroids and the Moon: the absolute magnitude H, coefficients G_{12}, G_1, and G_2, phase integral q, opposition-effect amplitude $\zeta - 1$, and the photometric slope k, all with two-sided 99.7% (or 3σ) errors. On the final row, we give the rms-values of the individual fits. For the Moon, the rms-value describes the residuals for 0–100° in phase angle.

	(24) Themis	(44) Nysa	(69) Hesperia	(82) Alkmene	(133) Cyrene	(419) Aurelia	(1862) Apollo	Moon
H (mag)	7.121	6.896	6.987	8.187	7.882	8.514	16.209	−0.124
	−0.042	−0.041	−0.036	−0.032	−0.026	−0.074	−0.022	−0.020
	+0.044	+0.044	+0.040	+0.034	+0.070	+0.052	+0.023	+0.022
G_{12}	0.68	−0.066	0.41	0.30	0.20	1.04	0.334	0.358
	−0.23	−0.077	−0.21	−0.14	−0.51	−0.46	−0.077	−0.073
	+0.25	+0.072	+0.26	+0.19	+0.49	+0.16	+0.077	+0.073
G_1	0.67	0.012	0.41	0.30	0.212	1.01	0.339	0.363
	−0.22	−0.058	−0.20	−0.13	−0.038	−0.44	−0.074	−0.069
	+0.24	+0.054	+0.25	+0.18	+0.463	+0.15	+0.073	+0.069
G_2	0.14	0.690	0.30	0.38	0.435	−0.079	0.353	0.338
	−0.15	−0.069	−0.16	−0.11	−0.297	−0.099	−0.047	−0.044
	+0.14	+0.074	+0.13	+0.10	+0.049	+0.282	+0.047	+0.044
q	0.395	0.573	0.424	0.437	0.447	0.356	0.4325	0.4298
	−0.027	−0.034	−0.028	−0.020	−0.053	−0.018	−0.0083	−0.0079
	+0.025	+0.036	+0.024	+0.032	+0.024	+0.050	+0.083	+0.0079
$\zeta - 1$	0.24	0.424	0.39	0.471	0.545747	0.073	0.444	0.427
	−0.12	−0.032	−0.15	−0.125	−0.314549	−0.060	−0.053	−0.049
	+0.13	+0.031	+0.15	+0.075	+0.000011	+0.217	+0.057	+0.052
k (°)$^{-1}$	−0.0292	−0.0104	−0.0234	−0.0204	−0.0177	−0.0353	−0.0214	−0.0221
	−0.0044	−0.0019	−0.0057	−0.0047	−0.0117	−0.0022	−0.0020	−0.0018
	+0.0049	+0.0019	+0.0058	+0.0041	+0.0015	+0.0081	+0.0021	+0.0019
rms (mag)	0.016	0.009	0.042	0.028	0.028	0.011	0.029	0.016

(typically asteroids with low geometric albedos), intermediate (intermediate albedos), and shallow photometric slopes (high albedos). Note that it is Deimos that is located in between the clusters in the middle and to the right. The G_1, G_2 relation in Fig. 6 can now be utilized in the development of a nonlinear two-parameter phase function, where the first parameter relates to the H magnitude and the second parameter describes the shape of the phase function. It is important to note that this "low-noise" G_1, G_2 relation is allowed for by the linear dependences of $\Phi_1(\alpha)$ and $\Phi_2(\alpha)$ at phase angles $\alpha \leqslant 7.5°$.

3.4. H, G_{12} phase function with application

The main reason to search for a two-parameter phase function is that, in the vast majority of cases, the goal is to derive reliable values for the absolute magnitude H from generally very poorly sampled phase curves. The three-parameter phase function lacks the predictive power to do so. In order to derive the two-parameter magnitude phase function, we express G_1 and G_2 in the H, G_1, G_2 phase function using a single nonlinear parameter G_{12}, that is,

$$\begin{aligned} G_1 &= G_1(G_{12}), \\ G_2 &= G_2(G_{12}). \end{aligned} \tag{25}$$

In the two-parameter H, G_{12} magnitude phase function, the reduced observed magnitudes can then be obtained from

$$10^{-0.4V(\alpha)} = L_0[G_1\Phi_1(\alpha) + G_2\Phi_2(\alpha) + (1 - G_1 - G_2)\Phi_3(\alpha)], \tag{26}$$

where L_0 is the disk-integrated brightness at zero phase angle and where we express G_1 and G_2 using the single parameter G_{12}. The absolute magnitude H is

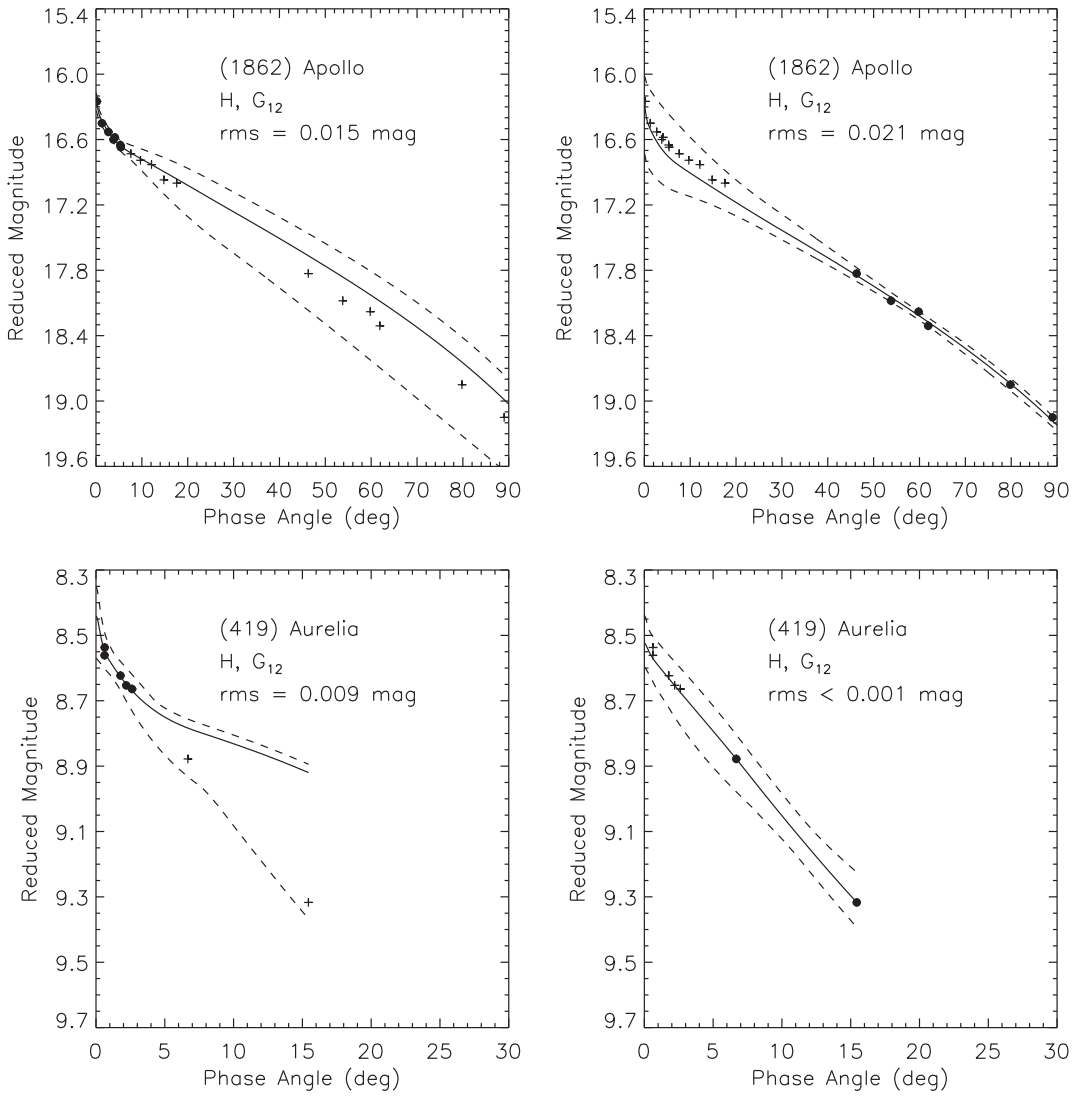

Fig. 8. Predictive power of the H, G_{12} magnitude phase function for (1862) Apollo and (419) Aurelia: the observations illustrated using solid bullets are included in the nonlinear least-squares solution and subsequent Monte-Carlo error analysis, whereas the observations illustrated using plus-signs serve as control points for predictive power. The dashed lines give the 99.7% error envelopes for the predictions.

$$H = -2.5\log_{10} L_0, \tag{27}$$

and the basis functions Φ_1, Φ_2, and Φ_3 are those of the H, G_1, G_2 magnitude phase function.

Here we present G_1 and G_2 as piecewise linear functions of G_{12}, relying on the G_1, G_2 relation in Fig. 6. We optimize the piecewise linear relationships using the observational data from five groups I–V (Tables 1 and 2), keeping the basis functions Φ_1, Φ_2, and Φ_3 fixed. Once the optimized relationships are available, the coefficients L_0 and G_{12} are estimated from the observations by using the nonlinear least-squares method or by a sequence of linear least-squares solutions as a function of the nonlinear parameter G_{12} (see Section 2.3). Note that the piecewise linear model is but one possible nonlinear model that can be utilized. After determining L_0 and G_{12}, H, G_1, and G_2 follow from the nonlinear relations in Eqs. (27) and (25).

The optimizations yields the following result with the m-metric value of $m = 0.0196$ mag which is almost as good as that of the H, G_1, G_2 magnitude phase function ($m = 0.0188$ mag):

$$\begin{aligned} G_1 &= \begin{cases} 0.7527G_{12} + 0.06164, & G_{12} < 0.2, \\ 0.9529G_{12} + 0.02162, & G_{12} \geqslant 0.2, \end{cases} \\ G_2 &= \begin{cases} -0.9612G_{12} + 0.6270, & G_{12} < 0.2, \\ -0.6125G_{12} + 0.5572, & G_{12} \geqslant 0.2. \end{cases} \end{aligned} \tag{28}$$

The full range of phase-function shapes is illustrated in Fig. 7 and the G_1, G_2 relation is described in Fig. 6. The phase functions intersect at $\alpha \approx 120^\circ$ (Fig. 7), where the H, G_1, G_2 basis functions Φ_1 and Φ_2 intersect. Studying the reason for the intersection in detail is beyond the scope of the present work. In Table 7, we show the resulting parameter and their error estimates for the same objects that were utilized to illustrate the H, G_1, G_2 phase function. The rms-values of the fits are almost as good as when using the H, G_1, G_2 phase function and the parameter error estimates are smaller.

In Fig. 8, we illustrate the predictive power of the H, G_{12} magnitude phase function for (1862) Apollo and (419) Aurelia. The two-parameter phase function produces acceptable predictions for both objects in two directions, that is, from small to large phase angles and vice versa. First, in three cases out of four, the prediction based on the best-fit curve accurately traces the observations excluded from the fit. Second, in all cases, the error envelopes are realistic and the observations excluded are well within the envelopes.

4. Conclusions

We have developed a three-parameter cubic-spline H, G_1, G_2 magnitude phase function for asteroids that provides excellent fits

to magnitude-phase observations. We have shown that this three-parameter phase function succeeds in removing the inability of the H, G magnitude phase function to adequately fit the phase curves of high-albedo and low-albedo asteroids. Furthermore, the H, G_1, G_2 phase function has allowed for the development of the nonlinear two-parameter H, G_{12} phase function that provides predictive power for small numbers of observations (sparse observational data) better than the H, G phase function.

We point out that, should a new type of asteroid photometric phase-curve data become available, it is possible to revise the magnitude phase functions using the methods currently presented. Finally, the new phase functions can turn useful in the interpretation of Gaia and Pan-STARRS photometry of asteroids.

Acknowledgments

The authors want to express their gratitude to ISSI (International Space Science Institute) for providing financial and logistical support to work together on light-scattering problems, as an ISSI International Team. The friendly and collaborative attitude of the ISSI staff during two meetings in Bern in January and December, 2008, is also acknowledged. The authors are thankful to A.W. Harris (Space Science Institute, Boulder, Colorado) and an anonymous reviewer for valuable comments on the manuscript. K. Muinonen's research has been partially supported by the EU/TMR project entitled "European Leadership in Space Astrometry" (ELSA), Academy of Finland (Project No. 127461), and he appreciates the helpful discussions with K. Lumme and H. Karttunen. A. Cellino's work was supported by the Italian space Agency (ASI), under Contract No. I/015/07/0. M. Delbò carried out part of this research while he was Henri Poincaré Fellow at the Observatoire de la Côte d'Azur. The Henri Poincaré Fellowship is funded by the CNRS-INSU, the Conseil General des Alpes-Maritimes and the Rotary International – District 1730. E. Tedesco's participation in this effort was supported through NASA Subcontracts Nos. 1324163 and 1384946 under JPL's NASA prime contract task order No. NMO7108563. The authors are thankful to S. Fornasier for providing information, prior to publication, on the phase curve of (2867) Steins observed by the ESA Rosetta space mission.

References

Belskaya, I.N., Shevchenko, V.G., Kiselev, N.N., Krugly, Yu.N., Shakhovskoy, N.M., Efimov, Yu.S., Gaftonyuk, N.M., Cellino, A., Gil-Hutton, R., 2003. Opposition polarimetry and photometry of S and E-type asteroids. Icarus 166, 276–284.

Bowell, E.G., Hapke, B., Domingue, D., Lumme, K., Peltoniemi, J., Harris, A.W., 1989. Application of photometric models to asteroids. In: Gehrels, T., Matthews, M.T., Binzel, R.P. (Eds.), Asteroids II. University of Arizona Press, pp. 524–555.

Cellino, A., Tanga, P., Dell'Oro, A., Hestroffer, D., 2007. Asteroid science with Gaia: Sizes, spin properties, overall shapes and taxonomy. Adv. Space Res. 40, 202–208.

Cellino, A., Dell'Oro, A., Tedesco, E.F., 2009. Asteroid families: Current situation. Planet. Space Sci. 57, 173–182.

Chernova, G.P., Lupishko, D.F., Shevchenko, V.G., Kiselev, N.N., Salies, R., 1991. Photometry and polarimetry of Asteroid 47 Aglaja. Kinematika Fiz. Nebesnykh Tel 7, N 5, 20–26.

Durda, D.D., Greenberg, R., Jedicke, R., 1998. Collisional models and scaling laws: A new interpretation of the shape of the main-belt asteroid size distribution. Icarus 135, 431–440.

Gehrels, T., 1956. Photometric studies of asteroids: V. The lightcurve and phase function of 20 Massalia. Astrophys. J. 123, 331–335.

Gehrels, T., Taylor, R.C., 1977. Minor planets and related objects: XXII. Phase function for 6 Hebe. Astron. J. 82, 229–232.

Gilks, W.R., Richardson, S., Spiegelhalter, D.J., 1996. Markov Chain Monte Carlo in Practice. Chapman & Hall/CRC, London.

Harris, A.W., Young, J.W., 1988. Two dark asteroids with very small opposition effects. Lunar Planet. Sci. XIX (2), 447–448.

Harris, A.W., Young, J.W., 1989. Asteroid lightcurve observations from 1979–1981. Icarus 81, 314–364.

Harris, A.W., Carlsson, M., Young, J.W., Lagerkvist, C.-I., 1984a. The lightcurve and phase relation of the Asteroid 133 Cyrene. Icarus 58, 246–256.

Harris, A.W., Young, J.W., Scaltriti, F., Zappala, V., 1984b. The lightcurve and phase relation of the Asteroids 82 Alkmene and 444 Gyptis. Icarus 57, 251–258.

Harris, A.W., Young, J.W., Goguen, J., Hammel, H.B., Hahn, G., Tedesco, E.F., Tholen, D.J., 1987. Photoelectric lightcurves of the Asteroid 1862 Apollo. Icarus 70, 246–256.

Harris, A.W., and 10 colleagues, 1989a. Photoelectric observation of Asteroids 3, 24, 60, 261, 863. Icarus 77, 171–186.

Harris, A.W., and 11 colleagues, 1989b. Phase relations of high albedo asteroids: The unusual opposition brightening of 44 Nysa and 64 Angelina. Icarus 81, 365–374.

Jedicke, R., Larsen, J., Spahr, T., 2002. Observational selection effects in asteroid surveys. In: Bottke, W.F., Cellino, A., Paolicchi, P., Binzel, R.P. (Eds.), Asteroids III. University of Arizona Press, pp. 71–87.

Jurić, M., and 15 colleagues, 2002. Comparison of positions and magnitudes of asteroids observed in the Sloan Digital Sky Survey with those predicted for known asteroids. Astron. J. 124, 1776–1787.

Muinonen, K., Piironen, J., Shkuratov, Yu.G., Ovcharenko, A., Clark, B.E., 2002. Asteroid photometric and polarimetric phase effects. In: Bottke, W.F., Cellino, A., Paolicchi, P., Binzel, R.P. (Eds.), Asteroids III. University of Arizona Press, pp. 123–138.

Pang, K.D., Rhoads, J.W., Hanover, G.A., Lumme, K., Bowell, E., 1983. Interpretation of whole-disk photometry of Phobos and Deimos. J. Geophys. Res. 88, 2475–2485.

Parker, A., Ivezić, Z., Jurić, M., Lupton, R., Sekora, M.D., Kovalski, A., 2008. The size distributions of asteroid families in the SDSS Moving Object Catalog 4. Icarus 198, 138–155.

Poutanen, M., Bowell, E., Martin, L.J., Thompson, D.T., 1985. Photoelectric photometry of Asteroid 69 Hesperia. Astron. Astrophys. Suppl. Ser. 61, 291–297.

Press, W.H., Teukolsky, S.A., Vetterling, W.T., Flannery, B.P., 1992. Numerical Recipes in Fortran. The Art of Scientific Computing, second ed. Cambridge University Press.

Shevchenko, V.G., 1997. Analysis of asteroid brightness phase relations. Solar Syst. Res. 31, 219–224.

Shevchenko, V.G., Chiorny, V.G., Kalashnikov, A.V., Krugly, Yu.N., Mohamed, R.A., Velichko, F.P., 1996. Magnitude-phase dependences for three asteroids. Astron. Astrophys. Suppl. Ser. 115, 1–6.

Shevchenko, V.G., Belskaya, I.N., Chiorny, V.G., Piironen, J., Erikson, A., Neukum, G., Mohamed, R., 1997. Asteroid observations at low phase angles. I. 50 Virginia, 91 Aegina and 102 Miriam. Planet. Space Sci. 45, 1615–1623.

Shevchenko, V.G., Belskaya, I.N., Krugly, Yu.N., Chiorny, V.G., Gaftonyuk, N.M., 2002. Asteroid observations at low phase angles. II. 5 Astraea, 75 Eurynome, 77 Frigga, 105 Artemis, 119 Althaea, 124 Alkeste and 201 Penelope. Icarus 155, 365–374.

Shevchenko, V.G., Chiorny, V.G., Gaftonyuk, N.M., Krugly, Yu.N., Belskaya, I.N., Tereschenko, I.A., Velichko, F.P., 2008. Asteroid observations at low phase angles. III. Brightness behavior of dark asteroids. Icarus 196, 601–611.

Tedesco, E.F., 1986. Ground-based data for asteroids and comets. In: Matson, D. (Ed.), IRAS Asteroid and Comet Survey: Preprint Version, vol. 1, pp. 9:1–9:42 (JPL Document No. D-3698).

Tedesco, E.F., Desert, F.-X., 2002. The infrared space observatory deep asteroid search. Astron. J. 123, 2070–2082.

Tedesco, E.F., Noah, P.V., Noah, M., Price, S.D., 2002a. The supplemental IRAS minor planet survey. Astron. J. 123, 1056–1085.

Tedesco, E.F., Egan, M.P., Price, S.D., 2002b. The midcourse space experiment infrared minor planet survey. Astron. J. 124, 583–591.

Tedesco, E.F., Cellino, A., Zappal, V., 2005. The statistical asteroid model. I. The main-belt population for diameters greater than 1 kilometer. Astron. J. 129, 2869–2886.